# Single-channel quantum-defect theory for the description of doubly excited states of helium

J. Q. Sun and C. D. Lin
*Department of Physics, Kansas State University, Manhattan, Kansas 66506-2601*
(Received 20 September 1991; revised manuscript received 23 June 1992)

A single-channel quantum-defect theory for the doubly excited states of helium is formulated in hyperspherical coordinates. For doubly excited states associated with each excited $He^+(N)$ threshold, the outer electron experiences asymptotically a combined Coulomb and dipole potential, $-1/R + \alpha/R^2$. The two independent solutions in the asymptotic region for energies below and above the threshold are explicitly given for both the attractive and the repulsive dipole potentials. Quantum defects for $^1P^\circ$ doubly excited states of the five channels in the $N = 3$ manifold and of the dominant channels below the $N = 2$, 3 and 4 thresholds of $He^+$ are calculated in a single-channel hyperspherical potential, and the results are compared with quantum defects extracted from other theoretical calculations and recent experimental results. Procedures for obtaining diabatic curves from the adiabatic potentials are also discussed.

PACS number(s): 31.50.+w, 32.80.Dz, 31.20.Tz

## I. INTRODUCTION

Over the years, the quantum-defect theory (QDT) [1] has been shown to be the most powerful method for treating the structure of Rydberg states of atoms and positive ions. It has been generalized [2, 3] to the multichannel problems to deal with the spectra of complex atoms. In the quantum-defect theory, one takes advantage of the fact that in the asymptotic region the outer electron experiences a Coulomb potential and its wave function can be expressed as a linear combination of the regular and irregular Coulomb functions. The mixing coefficient is related to the quantum defect (or scattering phase shift) which can be obtained either empirically [4] or by solving the many-electron problem [5] in the inner region.

In this article, we are interested in calculating the quantum defects of doubly excited states of helium converging to an excited $He^+$ threshold. It is well known [6] that the outer electron in these states experiences a dipole potential $\alpha/r^2$ in addition to the Coulomb potential $-1/r$, where $r$ is the radial distance of the outer electron from the nucleus. The coefficient $\alpha$ can be either positive or negative. When $\alpha$ is less than $-\frac{1}{4}$, one needs to treat the two independent solutions of the potential $-1/r + \alpha/r^2$ carefully. Otherwise, the two solutions are complex functions and the resulting complex quantum defect has discontinuity across the ionization threshold [2, 7]. A pair of such independent solutions have been obtained by Greene *et al.* [8]. In this paper we give an alternative pair which are more concisely expressed and easier to calculate.

In helium, for each $L$, $S$, and $\pi$ there are a number of channels (or Rydberg series) converging to each excited $He^+$ threshold. It has been shown [9, 10] from the hyperspherical treatment that to a first-order approximation, each Rydberg series is associated with an adiabatic hyperspherical potential curve. In this article, we will calculate the quantum defects for doubly excited $^1P^\circ$ Rydberg series in helium.

To carry out such calculations, a number of approximations have to be made. To begin with, it is known [11] that each hyperspherical channel couples to other channels asymptotically with a coupling proportional to $1/R$. This undesirable long-range coupling is related to the fact that in the asymptotic region the hyperspherical coordinates are not suitable for describing two independent electrons. The "spurious" coupling will vanish if independent-electron coordinates are used. In this article we neglect such coupling, under the assumption that the hyperradius and the radial distance of the outer electron is the same in the asymptotic region. This assumption can be removed in the future by matching the hyperspherical solutions in the large $R$ region to wave functions expressed in independent-particle coordinates [12].

The other consideration is the local diabatic treatment of the adiabatic potentials. It is known that there are sharply avoided crossings in the calculated adiabatic hyperspherical potential curves. Since the diabatic curves preserve the nature of electron correlation, the physical channel is better represented by treating the avoided crossing diabatically. In most of the previous calculations [13–15], this procedure was obtained by simply interpolating the calculated potential curves and diabatic wave functions were not obtained. In this article, we give a brief description of the numerical procedure for obtaining diabatic curves, the details of which are given elsewhere [16].

To calculate doubly excited states converging to the high-$N$ $He^+$ thresholds, the relevant potential curves have to be calculated. Section II describes the methods with which these curves are calculated, after a summary of the hyperspherical approach is given. The procedure for obtaining diabatic curves is also outlined in this section. The quantum-defect theory for the combined Coulomb and dipole potential is described in Sec. III. Results for the quantum defects from the single-channel calculations are given in Sec. IV which are also compared to

 

recent experimental results measured using synchrotron radiation [17] and to results deduced from other theoretical calculations [18]. The limitations and further improvements of the present approach are addressed in Sec. V. Atomic units are used throughout this paper except that of energy, which is in rydbergs.

## II. CALCULATIONS OF DIABATIC HYPERSPHERICAL POTENTIAL CURVES

### A. Summary of the hyperspherical approach

Starting with the spherical coordinates $(r_1, \theta_1, \phi_1)$ and $(r_2, \theta_2, \phi_2)$ of the two electrons, the hyperspherical coordinates are obtained by replacing $r_1$ and $r_2$ by a hyperradius $R = (r_1^2 + r_2^2)^{1/2}$ and a hyperangle $\alpha = \tan^{-1}(r_2/r_1)$. The two sets of spherical angles and $\alpha$ are denoted altogether by $\Omega$. By treating $R$ as the slow variable, the two-electron wave function can be expanded as [10]

$$\Psi(R,\Omega) = \sum_{\mu} F_{\mu}^{n}(R)\Phi_{\mu}(R;\Omega)/(R^{5/2}\sin\alpha\cos\alpha), \qquad (1)$$

where $\mu$ identifies the channel and $n$ denotes the $n$th state within that channel. The channel function $\Phi_{\mu}(R;\Omega)$ satisfies the differential equation

$$\frac{1}{R^2}\left(-\frac{d^2}{d\alpha^2} + \frac{l_1^2}{\cos^2\alpha} + \frac{l_2^2}{\sin^2\alpha} + 2RC(\alpha,\theta_{12})\right)\Phi_{\mu}(R;\Omega) = U_{\mu}(R)\Phi_{\mu}(R;\Omega), \qquad (2)$$

where $C(\alpha,\theta_{12})$ is the effective charge which depends only on $\alpha$ and $\theta_{12}$, with the latter being the angle between the two electrons with respect to the nucleus. In Eq. (1) the hyperradial functions $F_{\mu}^{n}(R)$ satisfy the coupled equations,

$$\left(\frac{d^2}{dR^2} + \frac{1}{4R^2} - U_{\mu}(R) + W_{\mu\mu}(R) + E_n\right)F_{\mu}^{n}(R) + \sum_{\nu\neq\mu} W_{\mu\nu}(R)F_{\nu}^{n}(R) = 0, \qquad (3)$$

where the coupling terms $W_{\mu\nu}$ are defined as

$$W_{\mu\nu} = 2\left\langle \Phi_{\mu}\left|\frac{d}{dR}\right|\Phi_{\nu}\right\rangle\frac{d}{dR} + \left\langle \Phi_{\mu}\left|\frac{d^2}{dR^2}\right|\Phi_{\nu}\right\rangle . \qquad (4)$$

### B. The calculation of adiabatic potential curves

The partial differential Eq. (2) is solved by the eigenfunction expansion method,

$$\Phi_{\mu}(R;\Omega) = A\sum_{[l_1,l_2]} u_{l_1 l_2}^{\mu}(R;\alpha)Y_{l_1 l_2 LM}(\mathbf{r}_1,\mathbf{r}_2) \qquad (5)$$

where $A$ is the antisymmetrization operator and $Y_{l_1 l_2 LM}$ is the coupled orbital angular momentum wave function. The basis function $u_{l_1 l_2}^{\mu}$ is expanded as a linear combination of hyperspherical harmonics and analytical functions generalized from the asymptotic limit (large $R$) [10]. With such a basis set, Eq. (2) reduces to an eigenvalue equation at each $R$,

$$Hc_{\mu} = U_{\mu}(R)Sc_{\mu}, \qquad (6)$$

where $S$ is the overlap matrix, and $H$ is the Hamiltonian matrix. Diagonalization of Eq. (6) over a range of $R$ allows the construction of a family of potential curves for each symmetry with fixed $L$, $S$, and $\pi$. In the present work we are interested in high doubly excited states of $H^-$ and He. These states are associated with the excited states of H or $He^+$, where the principal quantum number $N \gg 1$. In this case the number of potential curves is quite large and there are numerous avoided crossings among the curves. A straightforward diagonalization of Eq. (6) using a large basis set, as those carried out by Sadeghpour and Greene [14], would result in a very complicated set of potential curves. To simplify the calculation and to be able to isolate the important channels, we carried out the diagonalization in two steps. First, Eq. (6) is solved in a fixed $(l_1 l_2)$ basis set. Thus a set of hyperspherical harmonics and analytical channel functions within each fixed $(l_1 l_2)$ is first used to diagonalize Eq. (6). In this step, potential curves which converge to *different* $N$ in the asymptotic limit do not exhibit any avoided crossings. The eigenfunctions thus calculated for different pairs of $(l_1 l_2)$ then serve as the new basis functions in the second diagonalization where only basis functions belonging to the same N in the asymptotic limit are included.

The two-step diagonalization procedure treats each $N$ manifold (defined for the curves which converge to the same $N$ limit at large $R$) separately. Thus potential curves converging to different $N$ are allowed to cross. On the other hand, curves within each $N$ do exhibit avoided crossings.

In the first-step diagonalization, the basis functions used are not orthogonal and there is the possibility of numerical instability due to the linear dependence of the basis set. The instability can be avoided [14] by first diagonalizing the overlap matrix $S$ with a unitary matrix $C$. Upon removing eigenfunctions whose eigenvalues are less than a prescribed value (0.0001 was used in this work), the new secular equation (6) becomes stable.

### C. Diabatic treatment at the local avoided crossing

In the present approach, adiabatic potential curves are obtained for those belonging to the same $N$ manifold. These adiabatic curves show localized avoided crossings characterized by large values of $P_{\mu\nu} = \langle\mu|d/dR|\nu\rangle$ between certain pairs $\mu$ and $\nu$. It is desirable to remove these sharp $P_{\mu\nu}$ by transforming to a diabatic representation. This procedure is often taken by practitioners in ion-atom collisions [19] where a transformation matrix $C$ is calculated by solving

$$\frac{dC}{dR} + PC = 0 \qquad (7)$$

with the boundary condition that

$$C \to I \quad \text{as} \quad R \to \infty. \tag{8}$$

Consider the two-channel problem. Let $U_1(R)$ and $U_2(R)$ be the two adiabatic potential curves and $\Phi_1(R;\Omega)$ and $\Phi_2(R;\Omega)$ be the two adiabatic functions. Transformation to a diabatic set $\phi_1(R;\Omega)$ and $\phi_2(R;\Omega)$ can be achieved by a matrix $C$ such that

$$\begin{pmatrix} \phi_1(R;\Omega) \\ \phi_2(R;\Omega) \end{pmatrix} = \begin{pmatrix} \cos[\epsilon(R)] & -\sin[\epsilon(R)] \\ \sin[\epsilon(R)] & \cos[\epsilon(R)] \end{pmatrix} \begin{pmatrix} \Phi_1(R;\Omega) \\ \Phi_2(R;\Omega) \end{pmatrix}, \tag{9}$$

where $\epsilon(R)$ depends on $R$. Under such a tranformation the diabatic potential curves and the off-diagonal potential matrix element are given by

$$U_1^d(R) = U_1(R)\cos^2[\epsilon(R)] + U_2(R)\sin^2[\epsilon(R)], \tag{10}$$

$$U_2^d(R) = U_1(R)\sin^2[\epsilon(R)] + U_2(R)\cos^2[\epsilon(R)], \tag{11}$$

$$U_{12}^d(R) = U_{21}^d(R) = [U_1(R) - U_2(R)]\cos^2[\epsilon(R)]\sin^2[\epsilon(R)]. \tag{12}$$

The boundary condition Eq. (8) guarantees that the two functions $\phi_1(R;\Omega)$ and $\phi_2(R;\Omega)$ are true diabatic in that $\langle \phi_1(R;\Omega)|d/dR|\phi_2(R;\Omega)\rangle = 0$ for the whole range of $R$. However, it has the undesirable feature that the resulting diabatic potentials in Eqs. (10) and (11) deviate substantially from the adiabatic curves outside the avoided crossing region [20] and that $P_{\mu\nu}$ has to be calculated with fine mesh points in the avoided crossing region. In this work, we prefer a diabatization only in the region $R_1 < R < R_2$ where the nonadiabatic coupling is large. The detail of this method is given elsewhere [16]. Here we only outline the idea behind this diabatic transformation procedure. To begin with one must determine the range $R_1 \le R \le R_2$ where local diabatic transformation is to be performed. We choose $R_1$ and $R_2$ such that the magnitude of $P_{12}$ within the $R_1 \le R \le R_2$ region is greater than a predetermined value, say, 0.05. Let $\Phi_1(R_2;\Omega)$ and $\Phi_2(R_2;\Omega)$ be the two adiabatic functions at $R_2$, and $\Phi_1'(R_1;\Omega)$ and $\Phi_2'(R_1;\Omega)$ be the same at $R_1$. We construct the two diabatic functions $\phi_1(R;\Omega)$ and $\phi_2(R;\Omega)$ in the $R_1 \le R \le R_2$ region as the linear combination of these four functions. The $R$-dependent coefficients are assumed to take simple functional forms, but the resulting diabatic states are subject to the conditions that they coincide with the adiabatic states at $R_1$ and $R_2$, and that the first-order and second-order derivatives (with respect to $R$) are also continuous at the boundaries. The diabatic states constructed in this way have nonzero $\langle \phi_1|\frac{d}{dR}|\phi_2\rangle$ in the $R_1 \le R \le R_2$ region. The off-diagonal potential coupling $U_{12}^d$ is also nonzero in this interval. However, both are quite small and both can be neglected in a single-channel approximation.

## III. QUANTUM-DEFECT THEORY OF THE COMBINED COULOMB AND DIPOLE POTENTIALS

To obtain the full solution of the two-electron problem the coupled equations (3) in hyperspherical coordinates have to be solved with proper boundary conditions. Since hyperspherical coordinates do not describe the asymptotic region exactly (where independent-particle coordinates are the proper ones) there exists weak nonadiabatic couplings between channels. To achieve higher accuracy one may need to match the solution in the outer region to wave functions expressed in the independent-particle coordinates. This is a task for future development. In this article, we will focus on solving the coupled equations (3) within the hyperspherical formulation. We assume that the nonadiabatic coupling terms can be neglected outside a certain hyperradius $R_0$.

For $R > R_0$ , the radial equation for each channel $\mu$ is

$$\left[-\frac{d^2}{dR^2} + \frac{\alpha_\mu}{R^2} - \frac{2(Z-1)}{R} - \frac{Z^2}{N^2} - E\right] F_\mu(R) = 0, \tag{13}$$

where the asymptotic expression of $-0.25/R^2 + U_\mu(R) - W_{\mu\mu}(R)$ is used and $\alpha_\mu$ is the dipole moment in that channel. In the close-coupling approximation, an equation identical to (13) is obtained (with $R$ replaced by the radial distance $r$ of the outer electron) if the equations are given in the dipole representation.

To apply multichannel quantum-defect theory (MQDT) to express the solution of the coupled equations (3), one needs to examine the two independent solutions of (13). A pair of such independent solutions has been given by Greene *et al.* [8]. Here we will give an alternative pair which is more concise and easier to implement in numerical calculations.

Let $\lambda = \sqrt{\alpha_\mu + 1/4}$, $\varepsilon = E + Z^2/N^2$, and $\rho = (Z-1)R$, and Eq. (13) can be expressed as

$$\left[\frac{d^2}{d\rho^2} - \frac{(\lambda - \frac{1}{2})(\lambda + \frac{1}{2})}{\rho^2} + \frac{2}{\rho} + \varepsilon\right] F_\mu(\rho) = 0, \tag{14}$$

where $\lambda - \frac{1}{2}$ is the effective angular momentum. This is identical to the radial equation of the hydrogen atom for a noninteger angular momentum. When $\alpha_\mu > -\frac{1}{4}$, $\lambda$ is real, otherwise $\lambda$ is imaginary.

According to Seaton [2], the two independent solutions of Eq. (14) are $y(\kappa,\lambda,z)$ and $y(\kappa,-\lambda,z)$, where

$$\varepsilon = -1/\kappa^2, \qquad z = 2\rho/\kappa \tag{15}$$

and

$$y(\kappa,x,z) = \frac{(\kappa z)^{x+1/2}\exp(-z/2)}{\Gamma(x+\frac{1}{2}-\kappa)} \times \sum_{n=0}^{\infty} \frac{\Gamma(x+\frac{1}{2}-\kappa+n)z^n}{\Gamma(2x+1+n)n!}. \tag{16}$$

It is convenient in the following discussion to define

$$A(\kappa,\lambda) = \frac{\Gamma(\kappa+\lambda+\frac{1}{2})}{\kappa^{2\lambda}\Gamma(\kappa-\lambda+\frac{1}{2})} \tag{17}$$

$$B(\varepsilon,\lambda) = \begin{cases} \frac{A(i/k,\lambda)}{1-e^{-2\pi/k}e^{-i2\pi(\lambda+1/2)}}, & \varepsilon = k^2 > 0; \\ A(\nu,\lambda), & \varepsilon = -1/\nu^2 < 0, \end{cases} \tag{18}$$

$$H(\varepsilon,\lambda)=\begin{cases}\frac{A(i/k,\lambda)}{e^{2\pi/k}e^{i2\pi(\lambda+1/2)}-1}, & \varepsilon>0;\\ A(\nu,\lambda), & \varepsilon<0.\end{cases} \tag{19}$$

We next consider the properties of these independent solutions.

$$s(\kappa,\lambda,z)=\frac{B(\varepsilon,\lambda)^{1/2}}{\sqrt{2}}y(\kappa,\lambda,z), \tag{20}$$

$$c(\kappa,\lambda,z)=-\frac{1}{\sqrt{2}B(\varepsilon,\lambda)^{1/2}}\left(\frac{A(\kappa,\lambda)\cos(2\pi\lambda)y(\kappa,\lambda,z)-y(\kappa,-\lambda,z)}{\sin(2\pi\lambda)}-iH(\varepsilon,\lambda)y(\kappa,\lambda,z)\right). \tag{21}$$

The functions $s(\kappa,\lambda,z)$ and $c(\kappa,\lambda,z)$ have the desirable asymptotic forms:
For $\varepsilon>0$

$$s(i/k,\lambda,z)\sim\left(\frac{1}{\pi k}\right)^{1/2}\sin(\xi),\qquad \rho\to\infty \tag{22}$$

$$c(i/k,\lambda,z)\sim\left(\frac{1}{\pi k}\right)^{1/2}\cos(\xi),\qquad \rho\to\infty \tag{23}$$

where

$$\xi=k\rho+\frac{1}{k}\ln(2k\rho)-\tfrac{1}{2}\pi(\lambda-\tfrac{1}{2})+\arg[\Gamma(\lambda+\tfrac{1}{2}-i/k)]. \tag{24}$$

For $\varepsilon<0$,

$$s(\nu,\lambda,z)=\frac{\sin[\pi(\nu-\lambda+\frac{1}{2})]}{(2\nu)^{1/2}\pi K(\nu,\lambda)}\left(\frac{2\rho}{\nu}\right)^{-\nu}\exp\left(\frac{\rho}{\nu}\right)-\cos[\pi\left(\nu-\lambda+\tfrac{1}{2}\right)]\times\left(\frac{\nu^3}{2}\right)^{1/2}K(\nu,\lambda)\left(\frac{2\rho}{\nu}\right)^{\nu}\exp\left(-\frac{\rho}{\nu}\right),\qquad \rho\to\infty \tag{25}$$

### A. $\lambda-\frac{1}{2}$ is real but not an integer

This corresponds to the case of a repulsive dipole potential. The two independent solutions of Eq. (14) can be cast into two new independent functions

$$c(\nu,\lambda,z)=\frac{\cos[\pi(\nu-\lambda+\frac{1}{2})]}{(2\nu)^{1/2}\pi K(\nu,\lambda)}\left(\frac{2\rho}{\nu}\right)^{-\nu}\exp\left(\frac{\rho}{\nu}\right)+\sin[\pi\left(\nu-\lambda+\tfrac{1}{2}\right)]\times\left(\frac{\nu^3}{2}\right)^{1/2}K(\nu,\lambda)\left(\frac{2\rho}{\nu}\right)^{\nu}\exp\left(-\frac{\rho}{\nu}\right),\qquad \rho\to\infty \tag{26}$$

$$K(\nu,\lambda)=[\nu^2\Gamma(\nu+\lambda+\tfrac{1}{2})\Gamma(\nu-\lambda+\tfrac{1}{2})]^{-1/2}. \tag{27}$$

### B. $\lambda$ is imaginary

This corresponds to having an attractive dipole potential. The two independent functions in Eqs. (20) and (21) become complex. This will result in a complex reaction matrix such that the MQDT parameters cannot be easily defined. Furthermore, the complex $s(\kappa,\lambda,\rho)$ and $c(\kappa,\lambda,\rho)$ functions make the numerical calculation very difficult.

When $\varepsilon<0$, it can be seen from Eqs. (20) and (21) that the correct Coulomb functions for imaginary $\lambda$ should be

$$s(\nu,\lambda,z)=\left[\frac{B(\varepsilon,\lambda)^{1/2}}{\sqrt{2}}y(\nu,\lambda,z)+\text{c.c.}\right]\Big/2\cos(\pi\lambda), \tag{28}$$

$$c(\nu,\lambda,z)=-\left[\frac{1}{\sqrt{2}B(\varepsilon,\lambda)^{1/2}}\left(\frac{A(\nu,\lambda)\cos(2\pi\lambda)y(\nu,\lambda,z)-y(\nu,-\lambda,z)}{\sin(2\pi\lambda)}-iH(\varepsilon,\lambda)y(\nu,\lambda,z)\right)+\text{c.c.}\right]\Big/2\cos(\pi\lambda), \tag{29}$$

where c.c. denotes complex conjugate. After a careful derivation, one can prove that Eq. (29) can be simplified as

$$c(\nu,\lambda,z)=-\left[\frac{B(\varepsilon,\lambda)^{1/2}}{\sqrt{2}}y(\nu,\lambda,z)-\text{c.c.}\right]\Big/2\sin(\pi\lambda). \tag{30}$$

Equations (28) and (30) can be rewritten as

$$s(\nu,\lambda,z)=\frac{\operatorname{Re}\left[B(\varepsilon,\lambda)^{1/2}y(\nu,\lambda,z)\right]}{\sqrt{2}\cosh[\pi\operatorname{Im}(\lambda)]}, \tag{31}$$

$$c(\nu,\lambda,z)=-\frac{\operatorname{Im}\left[B(\varepsilon,\lambda)^{1/2}y(\nu,\lambda,z)\right]}{\sqrt{2}\sinh[\pi\operatorname{Im}(\lambda)]}. \tag{32}$$

The asymptotic forms of $s(\kappa,\lambda,\rho)$ and $c(\nu,\lambda,\rho)$ are

$$s(\nu,\lambda,z)=\frac{\sin[\pi(\nu+\frac{1}{2})]}{(2\nu)^{1/2}\pi K(\nu,\lambda)}\left(\frac{2\rho}{\nu}\right)^{-\nu}\exp\left(\frac{\rho}{\nu}\right) -\cos[\pi(\nu+\tfrac{1}{2})]\times\left(\frac{\nu^3}{2}\right)^{1/2}K(\nu,\lambda)\left(\frac{2\rho}{\nu}\right)^{\nu}\exp\left(-\frac{\rho}{\nu}\right), \quad \rho\to\infty \tag{33}$$

$$c(\nu,\lambda,z)=\frac{\cos[\pi(\nu+\frac{1}{2})]}{(2\nu)^{1/2}\pi K(\nu,\lambda)}\left(\frac{2\rho}{\nu}\right)^{-\nu}\exp\left(\frac{\rho}{\nu}\right) -\sin[\pi(\nu+\tfrac{1}{2})]\times\left(\frac{\nu^3}{2}\right)^{1/2}K(\nu,\lambda)\left(\frac{2\rho}{\nu}\right)^{\nu}\exp\left(-\frac{\rho}{\nu}\right), \quad \rho\to\infty. \tag{34}$$

Similarly, one can find that the correct Coulomb functions for $\varepsilon>0$ are

$$s(i/k,\lambda,z)=-\frac{\mathrm{Re}\left[B(\varepsilon,\lambda)^{1/2}y(i/k,\lambda,z)\right]}{\sqrt{2}\cosh[\pi\,\mathrm{Im}(\lambda)+\beta(\varepsilon,\lambda)]}, \tag{35}$$

$$c(i/k,\lambda,z)=-\frac{\mathrm{Im}\left[B(\varepsilon,\lambda)^{1/2}y(i/k,\lambda,z)\right]}{\sqrt{2}\sinh[\pi\,\mathrm{Im}(\lambda)+\beta(\varepsilon,\lambda)]}, \tag{36}$$

where

$$\beta(\varepsilon,\lambda)=\tfrac{1}{4}\left[\ln\left(1+e^{-\pi[2/k+2\,\mathrm{Im}(\lambda)]}\right)-\ln\left(1+e^{-\pi[2/k-2\,\mathrm{Im}(\lambda)]}\right)\right]. \tag{37}$$

When $\varepsilon\to 0$, $\beta(\varepsilon,\lambda)\to 0$.

The functions in Eqs. (35) and (36) have the same asymptotic forms as those in Eqs. (22) and (23) except for the expression of the phase

$$\xi=k\rho+\frac{1}{k}\ln(2k\rho)+\tfrac{1}{4}\pi+\tfrac{1}{2}\{\arg[\Gamma(\lambda+\tfrac{1}{2}-i/k)] -\arg[\Gamma(\lambda+\tfrac{1}{2}+i/k)]\}. \tag{38}$$

The two independent solutions, $f$ and $g$, given by Greene *et al.* [8] can be connected to $s$ and $c$ by a unitary transformation matrix, e.g.,

$$\begin{pmatrix} f \\ -g \end{pmatrix}=\begin{pmatrix} \cos\phi & \sin\phi \\ -\sin\phi & \cos\phi \end{pmatrix}\begin{pmatrix} s \\ c \end{pmatrix} \tag{39}$$

when $\lambda$ is real, $\phi=0$. When $\lambda$ is imaginary,

$$\phi=\begin{cases} -\tan^{-1}\{\tanh[\pi\,\mathrm{Im}(\lambda)]\arg[B(\varepsilon,\lambda)^{1/2}/\Gamma(1+2\lambda)]\}, & \varepsilon<0 \\ -\tan^{-1}\{\tanh[\pi\,\mathrm{Im}(\lambda)+\beta(\varepsilon,\lambda)]\arg[B(\varepsilon,\lambda)^{1/2}/\Gamma(1+2\lambda)]\}, & \varepsilon>0 \end{cases} \tag{40}$$

where $\phi$ is well described by $\phi=\phi_0+\phi_1\varepsilon$ for Rydberg states.

For a single-channel problem, if the quantum defect induced by the short-range interaction is $\mu_s$, the hyperradical wave function is

$$F(\rho)=\cos(\pi\mu_s)s(\kappa,\lambda,z)+\sin(\pi\mu_s)c(\kappa,\lambda,z). \tag{41}$$

Using the boundary condition at $\rho\to\infty$, the effective principal quantum number of a discrete state of the channel is given by

$$\nu_n=n-\mu_s-\mathrm{mod}[\tfrac{1}{2}-\mathrm{Re}(\lambda)]. \tag{42}$$

Thus there is an additional quantum defect $\mu_d=\mathrm{mod}[\frac{1}{2}-\mathrm{Re}(\lambda)]$ induced by the dipole potential. When $\lambda$ is imaginary, this additional quantum defect is $\frac{1}{2}$.

For a multichannel problem, the transform matrix $U_{\mu\alpha}$ and eigenquantum defects $\mu_\alpha$, where $\alpha$ denotes the eigenchannels in the small $R$ region, can be obtained by the standard QDT procedure. The bound states are then determined by the equation

$$\mathrm{Det}|U_{\mu\alpha}\sin\{\pi[\nu_\mu+\mathrm{Re}(\tfrac{1}{2}-\lambda_\mu)+\mu_\alpha]\}|=0. \tag{43}$$

## IV. RESULTS FOR $^1P^\circ$ DOUBLY EXCITED STATES OF He

### A. Diabatic curves

Using the two-step diagonalization method described in Sec. II, we have calculated the adiabatic potential curves for $^1P^\circ$ doubly excited states of He. In Fig. 1, the potential curves for all the channels that converge to $N\le 5$ of $He^+$ are shown. We define a $R$-dependent effective principal quantum number $n_\mu(R)$ where $U_\mu(R)=-Z^2/n_\mu^2(R)$, for each potential $U_\mu(R)$ (for He, $Z=2$). Thus $n_\mu(R)$ approaches the principal quantum number $N$ in the asymptotic limit, $R\to\infty$.

In the two-step diagonaliztion procedure, potential curves belonging to different manifolds were diagonalized separately and thus can cross, but curves within the same manifold were obtained in the same diagonalization and the resulting curves display avoided crossings, as can be seen in Fig. 1. The avoided crossings between the + and − curves are well known and the diabatization procedure can be applied to each pair of curves. In our calculation, the local diabatic treatment is carried out by selecting $R_1$ and $R_2$ in the $R_1<R<R_2$ region where

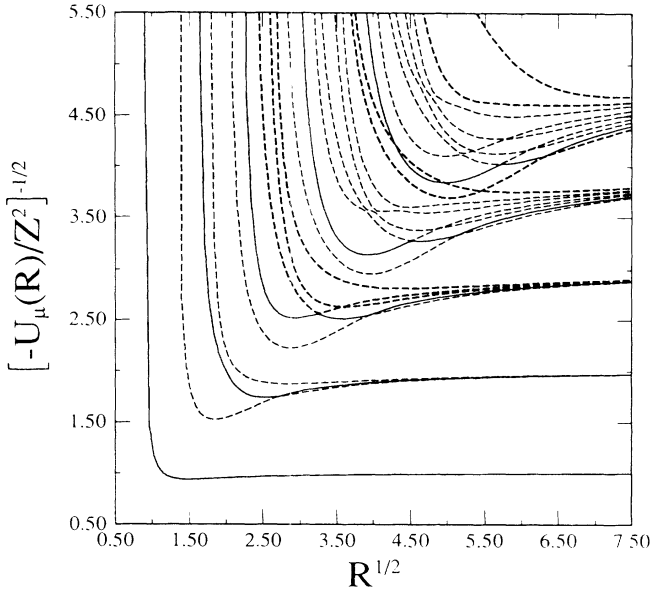


FIG. 1. Adiabatic potential curves for $^1P^\circ$ doubly excited states of He below the $N \leq 5$ thresholds of $He^+$. These curves are calculated using the two-step diagonalization procedure (see text) such that curves from different manifolds do not cross and those belonging to the same manifold show avoided crossings.

$$\left| \left\langle \Phi_\mu \left| \frac{d}{dR} \right| \Phi_\nu \right\rangle \right| \geq 0.05. \tag{44}$$

The resulting diabatic curves are shown in Fig. 2 where each curve can be labeled by the $K$, $T$ and $A$ quantum numbers [10]. It is noted that there still exist a number of sharply avoided crossings among the curves in the $N = 5$ manifold which were not treated diabatically.

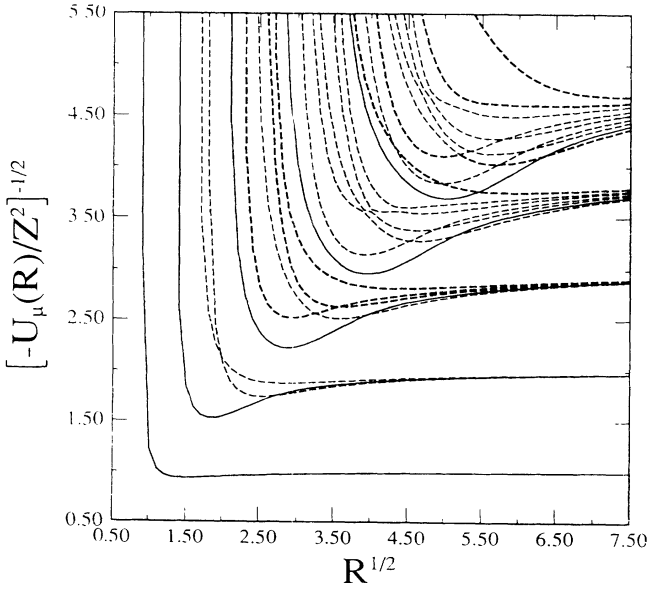


FIG. 2. Same as Fig. 1 except that each sharp avoided crossing within the same manifold has been transformed to a pair of diabatic curves.

### B. Calculations of quantum defects using one-channel hyperspherical potential curves for the $^1P^\circ$ states below the $N = 3$ threshold of $He^+$

The diabatic potential curves for the five $^1P^\circ$ channels that converge to the $N = 3$ threshold of $He^+$ are shown in an expanded scale in Fig. 3. Each channel can be labeled by the $K$, $T$, and $A$ quantum numbers. There are two $A = +1$ channels and two $A = -1$ channels and one $A = 0$ channel. For simplicity we use $1 + (-)$ to denote the lowest $+(-)$ channel and $2 + (-)$ the second $+(-)$ channel, and 0 to denote the $A = 0$ channel. The diabatic crossings between the $+$ and $-$ curves have been treated. These five channels are coupled by the nonadiabatic coupling terms among them. In principle, it is possible to calculate the MQDT parameters by solving the coupled equations (3) in the small-$R$ region and then match the solution in the outside region to the analytical Coulomb functions described in Sec. III.

In this article, our goal is to check the accuracy of quantum defects calculated using the one-channel approximation. Thus we solve a one-channel problem for each potential curve (but including the diagonal $W_{\mu\mu}$ term) and calculate the quantum defect for each channel. The results are summarized in Table I.

Recall that each potential curve takes the asymptotic form

$$U_\mu(R) = -\frac{Z-1}{R} + \frac{\alpha_\mu}{R^2}, \tag{45}$$

where $\alpha_\mu$ is the dipole moment. As explained in Sec. III, the quantum defect can be decomposed into two parts, $\mu = \mu_d + \mu_s$. Since the quantum defect varies slowly with energy, one can write $\mu_n$ for each state with energy $E_n$ by

$$\mu_n = \mu_0 + \mu_1(E_n - E_{\text{th}}) \tag{46}$$

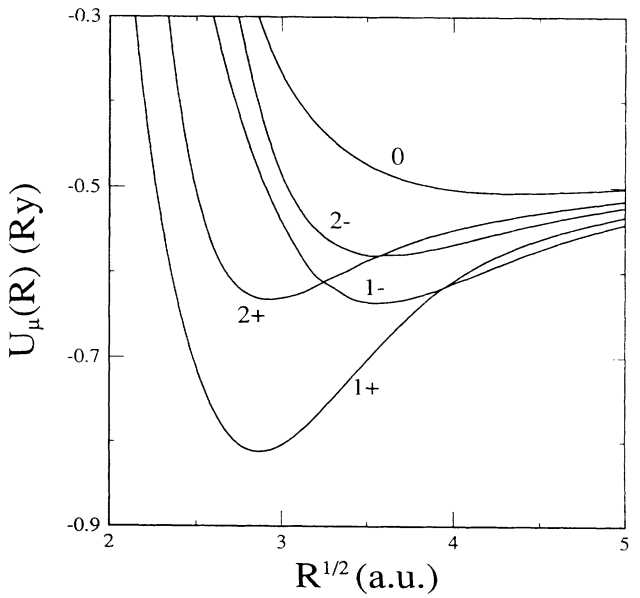


FIG. 3. The five diabatic curves for the $^1P^\circ$ doubly excited states that converge to the $N = 3$ threshold of $He^+$.

TABLE I. Dipole parameters and quantum defect parameters for the five $^1P^\circ$ channels of He that converge to the $N = 3$ threshold of $He^+$. Each channel is labeled with the $(K,T)^A$ quantum number, together with the dipole moment $\alpha$, the quantum defect from the dipole part, $\mu_d$. The quantum defect $\mu_0$ and its derivative $\mu_1$ are defined according to Eq. (46).

| | $(K,T)^A$ | $\alpha$ | $\mu_d$ | $\mu_0$ a | $\mu_0$ b | $\mu_0$ c | $\mu_0$ d | $\mu_1$ a |
|---|---|---|---|---|---|---|---|---|
| 1− | $(2,0)^-$ | −6.462 | 0.5 | 0.072 | 0.23 | 0.25 | 0.25 | −0.967 |
| 1+ | $(1,1)^+$ | −0.924 | 0.5 | 0.657 | 0.78 | 0.80 | 0.82 | −1.382 |
| 2− | $(0,0)^-$ | 4.804 | 0.252 | 0.133 | 0.26 | 0.57 | 0.60 | 2.096 |
| 2+ | $(-1,1)^+$ | 8.924 | 0.471 | 0.511 | 0.52 | 0.76 | 0.80 | −2.054 |
| 0 | $(-2,0)^0$ | 15.658 | 0.512 | 0.321 | 0.39 | 0.36 | 0.38 | −1.179 |

[a]Present results.
[b]Lipsky *et al.*, Ref. [18].
[c]Moccia and Spizzo, Ref. [21].
[d]Ho, Ref. [22].

where the energies are given in rydbergs, and $E_{\rm th}$ is the energy of the threshold. In Table I, the dipole moment $\alpha$ and the quantum defect $\mu_d$ from the dipole part for each channel are listed. The calculated quantum defect $\mu_0$ for each channel and its first-order derivative $\mu_1$ with respect to energy from a single hyperspherical channel are also shown, and the results are compared to those extracted from the calculations of Lipsky, Anania, and Conneely [18], and of Moccia and Spizzo [21], and of Ho [22]. The latter two calculations are much more elaborate, but even then the calculated quantum defects for the states cannot be easily fitted to Eq. (46). From the comparison one can draw the conclusion that the quantum defects extracted from the one-channel approximation are not quite adequate. To achieve higher accuracy, channel couplings should be included.

### C. Quantum defects along the double Rydberg series

Using the single-channel approximation, we have also calculated the quantum defects for the various doubly excited states of He converging to the various excited thresholds. These results are to compare with the quantum defects derived from recent high-resolution data of Domke *et al.* [17] using synchrotron radiation. For doubly excited states associated with $N \geq 5$ thresholds, experimental data show strong modulations in the observed spectra, indicating strong channel interactions due to states belonging to different manifolds. Thus we limit the calculation of single-channel quantum defects to the dominant channels below the $N = 4$ threshold. The results are summarized in Table II. We note that the quantum defects for the $N = 2$ and 3 channels are good to within about 0.1 as compared to those derived from the experimental data. For the $(2,1)^+$ channel associated with the $N = 4$ threshold, the discrepancy is quite large. It is not clear whether the difference is due to the channel couplings among the $N = 4$ manifold, or due to channel interactions with other manifolds. One needs to perform coupled-channel calculations in the future to resolve the origin of the discrepancy.

TABLE II. Calculated quantum defects $\mu_0$ and the derivatives $\mu_1$ with respect to energy obtained from a single hyperspherical channel potential. Notations are as in Table I where the experimental quantum defects $\mu_0^{\rm ex}$ are derived from Ref. [17].

| $N$ | $(K,T)^A$ | $\alpha$ | $\mu_d$ | $\mu_0^{\rm th}$ | $\mu_0^{\rm ex}$ | $\mu_1^{\rm th}$ |
|---|---|---|---|---|---|---|
| 2 | $(1,0)^-$ | −1.2 | 0.5 | 0.645 | 0.71 | −0.175 |
| 2 | $(0,1)^+$ | 2.0 | 0 | 0.041 | 0.147 | −0.624 |
| 3 | $(1,1)^+$ | −0.924 | 0.5 | 0.657 | 0.796 | −1.382 |
| 4 | $(2,1)^+$ | −6.836 | 0.5 | 0.849 | 0.351 | 1.870 |

## V. SUMMARY AND FUTURE DEVELOPMENTS

In this article we calculated the quantum defects of doubly excited states of helium using single-channel hyperspherical potential curves. Explicit expressions for the two independent solutions of the second-order differential equations in the combined Coulomb field and the dipole field are given. It is shown that the quantum defect can be decomposed into contributions from the dipole potential and from the remaining short-range interaction potential. The calculated quantum defects for each Rydberg series from a single hyperspherical channel are compared to those derived from experimental data and from other theoretical calculations. We showed that the single-channel results are acceptable but not adequate. Improvement on the present results would require a more careful inclusion of the coupling among the channels within the same manifold, and probably the coupling with channels in other manifolds as well.

We have discussed a procedure for transforming a pair of adiabatic potential curves into a pair of diabatic curves. The transformation is carried out only in the sharp avoided-crossing region such that the diabatic curves coincide with the adiabatic curves except in the narrow region where the transformation has been applied. Further discussion on this procedure is given elsewhere [16].

In closing we remark that a somewhat different approach may be needed in order to treat the channel cou-

plings among the hyperspherical channels. The present results reveal the inadequacy of approximating a Rydberg series by a single hyperspherical channel. The accuracy of the calculated quantum defects, while not unacceptable, are by no means comparable to the accuracy from the state-of-the-art results [21, 22]. The diabatic transformation discussed here applied to each pair of states locally only. In order to achieve high degree of accuracy, coupling among many channel may be needed. In the immediate future it is desirable to calculate quantum defects by including the couplings among the channels within the same manifold, for example, among the five channels in the $N = 3$ manifold. Couplings among channels belonging to different manifolds are needed for doubly excited states converging to the higher $N$ thresholds. The latter can be seen clearly from the recent experimental data where the Rydberg series for $N \geq 5$ show modulations due to the perturbation from isolated states belonging to higher manifolds [17]. Despite the deficiency of the one-channel approximation used in the numerical application, it should be emphasized that the quantum-defect theory presented in this article can be applied easily to multichannel cases and computational procedures for carrying out such calculations are being developed.

## ACKNOWLEDGMENTS

This work was supported in part by the U.S. Department of Energy, Division of Chemical Sciences. J.Q.S. thanks Z. Chen for helpful discussions. We also thank Chris Greene for making critical comments on the original manuscript.

[1] M. J. Seaton, Proc. Phys. Soc. (London) **88**, 801 (1966).
[2] M. J. Seaton, Rep. Prog. Phys. **46**, 167 (1983).
[3] U. Fano, Rep. Prog. Phys. **46**, 97 (1983). See also U. Fano and A. R. P. Rau, *Atomic Collisions and Spectra* (Academic, New York, 1986).
[4] K. T. Lu, Phys. Rev. A **4**, 579 (1971).
[5] C. M. Lee, Phys. Rev. A **10**, 584 (1974).
[6] I. C. Percival and M. J. Seaton, Proc. Cambridge Philos. Soc. **53**, 654 (1957).
[7] J. Dubau, J. Phys. B **7**, 2533 (1978).
[8] C. Greene, U. Fano, and G. Strinati, Phys. Rev. A **19**, 1485 (1979); C. H. Greene, A. R. P. Rau, and U. Fano, *ibid.* **26**, 2441 (1982).
[9] J. H. Macek, J. Phys. B **1**, 831 (1968).
[10] C. D. Lin, Adv. At. Mol. Phys. **22**, 77 (1986).
[11] J. H. Macek, Phys. Rev. A **31**, 2162 (1985).
[12] J. C. Light and R. B. Walker, J. Chem. Phys. **65**, 4272 (1976).
[13] C. D. Lin, Phys. Rev. Lett. **35**, 1150 (1975).
[14] H. R. Sadeghpour and C. H. Greene, Phys. Rev. Lett. **65**, 313 (1990).
[15] T. Motoyama, N. Koyama, and M. Matsuzawa, Phys. Rev. A **38**, 670 (1988).
[16] J. Q. Sun and C. D. Lin (unpublished).
[17] M. Domke *et al.*, Phys. Rev. Lett. **66**, 1306 (1991).
[18] L. Lipsky, R. Anania, and M. J. Conneely, At. Data Tables **20**, 127 (1977).
[19] T. G. Heil, S. E. Butler, and A. Dalgarno, Phys. Rev. A **23**, 1100 (1981).
[20] J. Tan and C. D. Lin, Phys. Rev. A **37**, 1152 (1988).
[21] R. Moccia and P. Spizzo, Phys. Rev. A **43**, 2199 (1991). This article also contains extensive survey of experimental and theoretical results for $^1P^\circ$ states of He below the $N = 2$ and 3 thresholds of $He^+$.
[22] Y. K. Ho, Phys. Rev. A **44**, 4154 (1991).